PROCEEDINGS OF SPIE

Additive manufacturing of titanium dioxide for dielectric photonic crystals

Andrey Vyatskikh, Ryan C. Ng, Bryce Edwards, Julia R. Greer

Additive Manufacturing of Titanium Dioxide for Dielectric Photonic Crystals

Andrey Vyatskikh[1,*], Ryan C. Ng[2], Bryce Edwards[1], Julia R. Greer[1]

[1]Division of Engineering and Applied Science, California Institute of Technology, Pasadena, CA 91125
[1]Division of Chemistry and Chemical Engineering, California Institute of Technology, Pasadena, CA 91125

ABSTRACT

Fabrication of 3D dielectric photonic crystals in the visible and in the infrared range typically requires sub-micron structural features and high-refractive index materials. We developed a template-free additive manufacturing (AM) process based on direct laser writing (DLW) that can create complex 3D architectures out of titania (TiO_2) with ~100 nm resolution. In this process, we synthesize hybrid organic-inorganic materials that contain titanium clusters coordinated with acrylic ligands to prepare a photoresist that is amenable to two-photon lithography (TPL). We sculpt a pre-ceramic architecture using TPL and then pyrolyze in air at 900°C to remove the organic constituents to produce a replica of the original structure with ~70% reduced linear dimensions. Energy-Dispersive Spectroscopy (EDS) and Raman spectroscopy confirm the constituent solid to consist predominantly out of rutile titania.

We demonstrate this process by fabricating titania woodpile structures with lateral dimensions of 70 x 70 μm and lateral periodicities between 1.0 and 1.3 μm. Fourier Transform Infrared (FTIR) spectroscopy reveals passive tuning of the reflectance peak between 1.7 and 2.3 μm, which agrees with Plane Wave Expansion simulations. This titania AM process offers a promising pathway to efficiently fabricate complex 3D nano-architectures out of a high-index material for 3D dielectric photonic crystals in the visible and the infrared.

Keywords: additive manufacturing, pre-ceramic polymer, titanium dioxide, titania, photonic crystal

1. INTRODUCTION AND BACKGROUND

Three-dimensional (3D) dielectric photonic crystals (PhCs) have been extensively studied for their unique ability to manipulate light, with some examples including PhCs with a full photonic bandgap[1,2] and negative refractive index materials[3]. Fabricating 3D dielectric PhCs in the visible and in the infrared generally requires a capability to 3D architect sub-micron features out of a low absorption, high refractive index material[4]. For example, a full photonic bandgap in woodpile structures can only be obtained with constituent materials possessing a refractive index n ≳1.9[5], and observing all-angle negative refraction in a 3D PhC proposed by Luo et al. requires an effective refractive index of n≥2.49[6]. Nano-architecting transparent high refractive index materials in 3D is technically challenging and requires complex experimental procedures, such as multi-angled etching[7], stacking individual layers using micromanipulation[8], or double-inversion of a 3D polymer template[2,4].

Additive manufacturing (AM) by laser-based lithography of hybrid organic-inorganic materials offers a promising pathway for facile fabrication of 3D PhCs in the visible and the infrared[9]. Several hybrid materials that can be used for lithography, including Si, Zr, Zn, and Ge-based compositions, have been formulated and demonstrated[10–12], but the refractive indices of the final materials have been found to be less than 1.6[10–12]. Titanium-based hybrid materials are promising candidates for fabrication of 3D PhCs in the visible and the infrared due to a high refractive index of titanium dioxide (TiO_2), but only 2D patterning of TiO_2/carbon composites has been demonstrated so far[13].

In this work, we demonstrate an AM process that is capable of producing sub-micron features out of titanium dioxide. We synthesize a hybrid organic-inorganic precursor of TiO_2 and, based on the precursor, formulate a pre-ceramic photoresist for two-photon lithography, which is used to fabricate a pre-ceramic part. The part is then pyrolyzed in air at

900°C, which yields a part consisting entirely out of rutile TiO$_2$. We demonstrate this process by fabricating titania woodpile fct structures and show that the measured reflectance peaks between 1.7 and 2.3 µm correspond to the positions of partial photonic bandgaps expected from plane wave expansion simulations for titania woodpiles. These findings suggest an efficient way of fabricating nano-architected 3D PhCs out of rutile TiO$_2$.

2. MATERIALS AND METHODS

Titanium (IV) ethoxide (>97%), acrylic acid (anhydrous, 99%), 2-methoxyethanol (anhydrous, 99.8%), pentaerythritol triacrylate (technical grade), dichloromethane (DCM) (anhydrous, ≥99.8%), and propylene glycol monomethyl ether acetate (PGMEA) (>99.5%) were purchased from Sigma Aldrich. We synthesized a titania precursor that is amenable to participating in a free-radical polymerization reaction using a ligand exchange reaction between titanium (IV) ethoxide and acrylic acid described in ref.[14] (Fig. 1a). Using this precursor, we formulated a hybrid organic-inorganic photoresist using an approach described in detail in ref.[15].
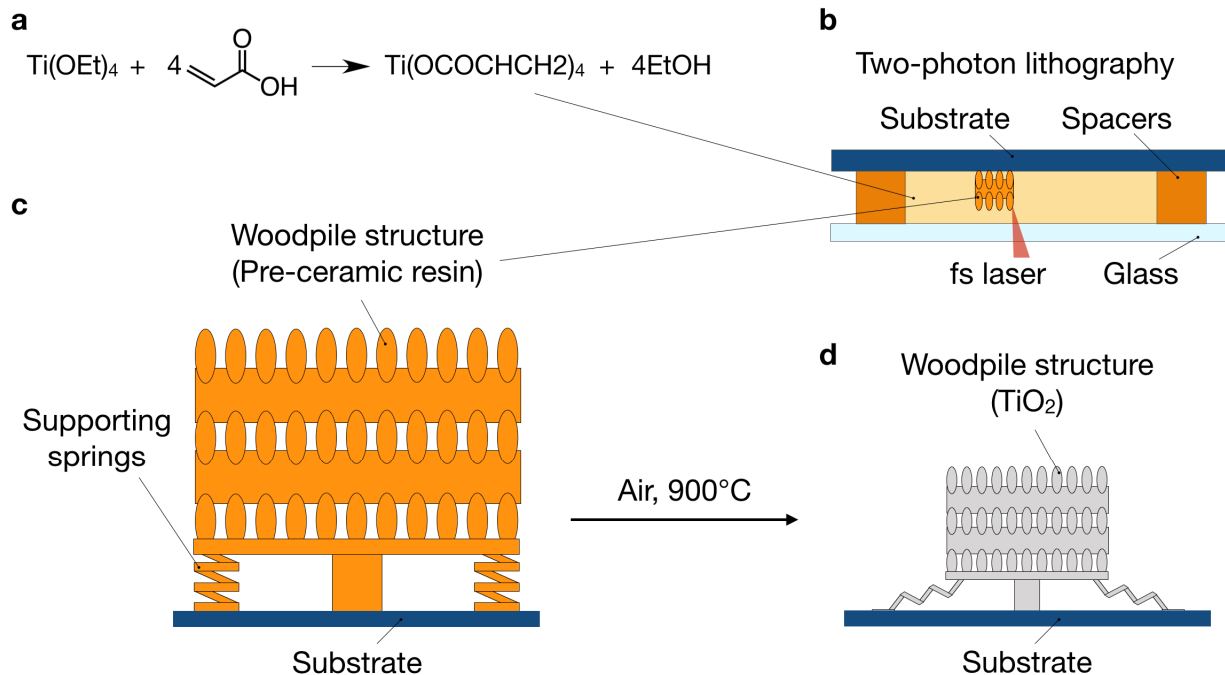

Figure 1. Process for AM of nano-architected titanium dioxide (TiO2). (a) Titania precursor is synthesized using a ligand exchange reaction between titanium (IV) ethoxide and acrylic acid. (b) Schematic of the assembly for sculpting the titania pre-ceramic photoresist into 3D architectures using two-photon lithography. (c) Schematic of a woodpile structure made out of a cross-linked pre-ceramic resin that is being pyrolyzed to form (d) the final nano-architected structure out of titania.

Samples were fabricated using a commercially available two-photon lithography system (Photonic Professional GT, Nanoscribe GmbH) (Fig. 1b) followed by a development procedure outlined in ref.[15]. The samples were then pyrolyzed in air in a tube furnace. The temperature was ramped up to 900°C at 2°C/min, kept at 900°C for 1 hour, and then the furnace was let to cool down at a natural rate.

SEM images were taken using FEI Versa 3D DualBeam. SEM Energy-Dispersive X-Ray Spectroscopy (EDS) characterization was conducted with Zeiss 1550VP FESEM equipped with Oxford X-Max SDD using a 10 kV electron beam. Raman spectrum was collected using Renishaw M1000 MicroRaman Spectrometer equipped with a 514.5 nm laser. Single crystalline rutile titania sample for a reference Raman spectrum was provided by Prof. George Rossman (crystal # GRR 1810).

Band structures were calculated using a plane wave expansion (PWE) method with a commercially available software package RSoft BandSOLVE. These simulations were performed for photonic crystals with face-centered tetragonal (fct) woodpile geometry having $n = 2.2$ for the constituent material and the ratio between the axial and the lateral periods of 1.1.

Reflectance spectra from the woodpile structures were collected using Nicolet iS50 FT-IR spectrometer equipped with a Nicolet Continuum Infrared Microscope and a calcium fluoride detector. The angle range for the Cassegrain objective used in the microscope was between 16° and 35.5° relative to the normal.

3. RESULTS

We synthesized a pre-ceramic titania photoresist and used it in a commercially available two-photon lithography machine to fabricate structures with fct woodpile geometry that had 15 layers in the axial direction, a lateral period of 3.9 μm, beams with 3.5 x 0.6 μm elliptical cross-sections, a ratio of the axial period to the lateral period of 1.1, and overall lateral dimensions of 250 x 250 μm (see Figs. 2a, b). These woodpile structures were placed on a set of springs and pillars that allowed it to effectively decouple the structure from the substrate (Fig. 2a) and maintain isotropic shrinkage during subsequent processing.
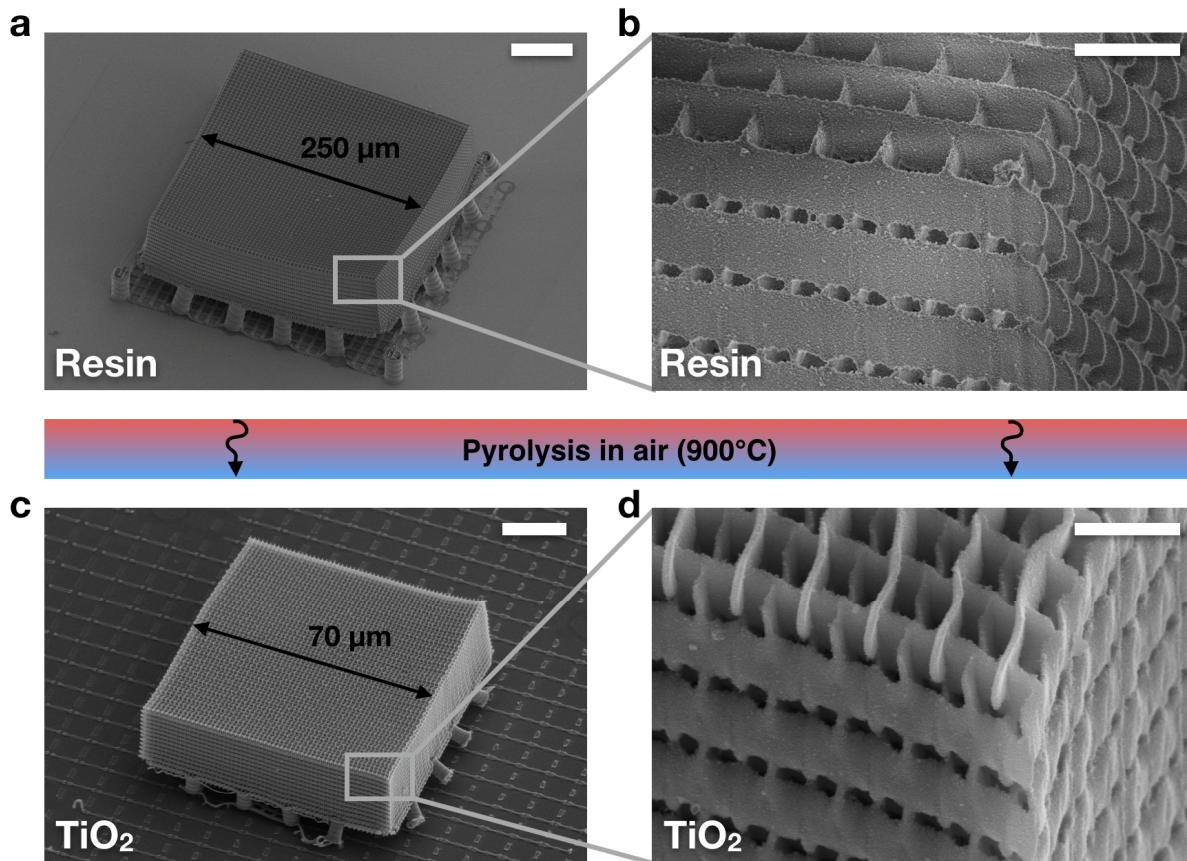

Figure 2. SEM images of a representative woodpile structure supported on a set of springs and pillars (a, b) before and (c, d) after the pyrolysis step of the AM process. Scale bars are 50 μm for (a), 5 μm for (b), 20 μm for (c), and 2 μm for (d).

The pyrolysis of samples in air at 900°C was accompanied by the removal of organic constituents of the pre-ceramic resin and a linear shrinkage of ~70%. A representative woodpile sample after pyrolysis is shown in Figs. 3c, d. SEM images of these woodpile structures show beams with 960 x 150 nm elliptical cross-sections, lateral periodicities of 1090 nm, and overall lateral dimensions of 70 x 70 μm. The features are uniformly sized and fully dense, and the shrinkage is

isotropic. SEM images also reveal that the top beams of the woodpile structure are buckled (see Fig. 2d), which stems from the lack of support of the top slender beams during the shrinkage compared to their counterparts that are closer to the substrate in the axial direction.

The chemical composition of as-fabricated structures was characterized using SEM EDS of a representative woodpile architecture with a lateral period of 1.1 μm (Fig. 3a). EDS maps shown in Figs. 3b-d reveal a homogeneous distribution of Ti and O throughout the structure. Oxygen presence on the substrate can be attributed to oxidation of the top layer of silicon during heat treatment in air at 900°C. EDS spectrum taken from a region within the woodpile structure (Fig. 3e) conveys that the constituent material consists predominantly out of Ti and O, which is consistent with the expected TiO_2 composition. Raman spectrum taken from the woodpile structure (Fig. 3f) showed a rutile TiO_2 signature. The comparison to a reference spectrum of single crystalline rutile titania is also shown in Fig. 3f.
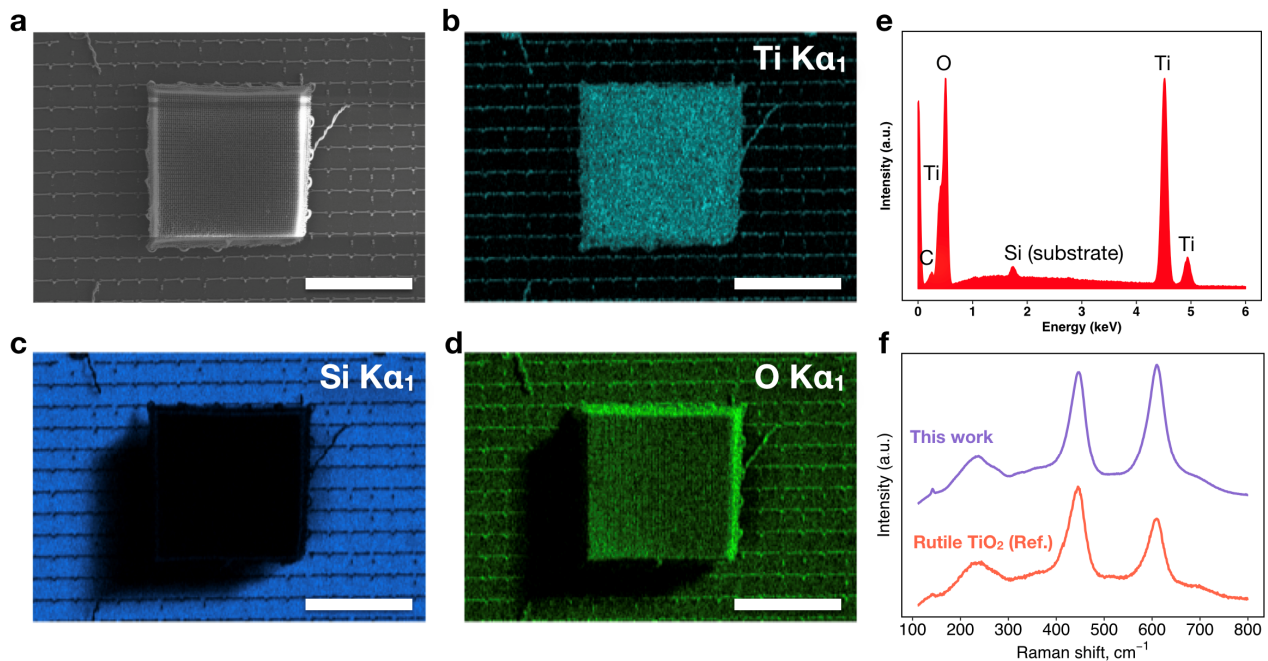

Figure 3. EDS and Raman characterization of as-fabricated TiO2 woodpiles. (a) SEM image of a woodpile structure on a silicon substrate (top view) where EDS maps were taken. (b-d) EDS maps of titanium, silicon, and oxygen showing uniform distribution of Ti and O throughout the woodpile structure. (e) EDS spectrum taken from the woodpile structure reveals mostly titanium and oxygen content. (f) Raman spectrum taken from the woodpile structure compared with a reference spectrum of rutile titania suggests a pre-dominant rutile phase of TiO_2. Scale bars are 50 μm for (a-d).

To determine the expected optical behavior of as-fabricated woodpile structures, we calculated a corresponding band structure using a PWE method and commercially available software. Figure 4a shows a band structure calculated for a woodpile structure with a lateral period of 1090 nm (Fig. 4b). The simulation revealed the emergence of a partial photonic bandgap in this woodpile structure. Due to the angle range of the Cassegrain objectives used for experimental measurements being limited to between 16° and 35.5°, we calculated the expected partial photonic bandgap positions for these angles from the band diagram, with normal incidence defined to be the ΓX direction. For 16°, the bandgap was calculated to be between 0.4907(2 πc/a) and 0.5127(2 πc/a) along X-U-L and between 0.4909(2 πc/a) and 0.5149(2 πc/a) along X-W-K. For 35.5°, the bandgap edges were calculated to be 0.5226(2 πc/a) and 0.5454(2 πc/a) along X-U-L and 0.5343(2 πc/a) and 0.5629(2 πc/a) along X-W-K.

Experimental measurements of the reflectance spectrum was conducted using FTIR (see Fig. 4c). FTIR revealed the emergence of a reflectance band centered at around 1.9 um. To compare these experimental results to theory, we plotted the range of the calculated bandgap positions for angles between 16° and 35.5° as vertical dash lines in Fig. 4c. We found an overall good fit between the range of calculated partial photonic bandgap positions (between 1940 and 2220 nm for a woodpile with a lateral period of 1090 nm) and the observed reflectance peak. Experimentally observed reflectance

peaks appear to be wider than the expected width of the partial bandgaps, which likely stems from fabrication imperfections contributing to the variation of periodicity in the woodpile structure along the axial direction.
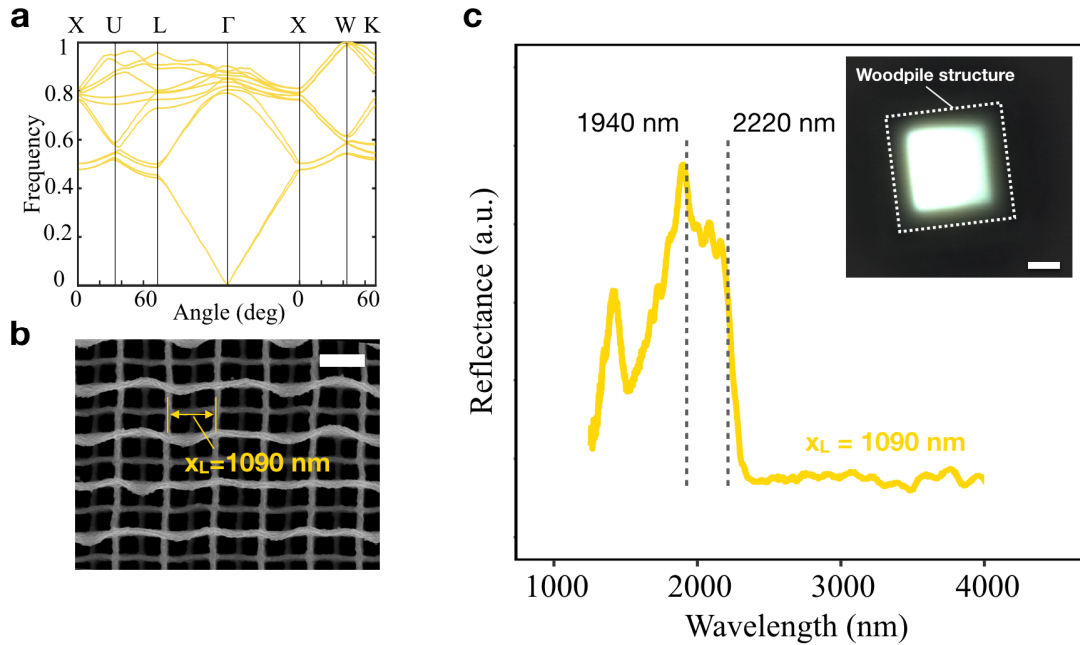

Figure 4. (a) Band structure of a woodpile architecture with a lateral period of 1090 nm showing the emergence of a partial band gap. (b) SEM of a representative woodpile structure (top view) with a lateral period of 1090 nm fabricated using this AM process. (c) Measured reflectance spectrum taken from the woodpile structure showing the emergence of a high reflectance band centered at around 1.9 um. Vertical dash lines indicate the range of partial gap edge positions calculated by PWE for the incident angles between 16° and 35.5° that were probed by FTIR in the experiment. The inset optical image shows a 50 x 50 μm area within the woodpile where the measurement was taken. Scale bars are 1 μm for (b) and 20 μm for (c)

To demonstrate the efficiency of this titania AM process for rapid prototyping of dielectric photonic crystals, we fabricated four woodpile architectures with lateral periodicities of 990 nm, 1090 nm, 1190 nm, and 1300 nm, the ratios between the axial periods and the lateral periods of 1.1, the number of lateral periods of 70, 64, 59, and 54, and the number of axial periods of 15, 15, 14, and 12, correspondingly. Figures 5a-d show band diagrams calculated for these architectures using PWE. Figures 5e-h show top views of as-fabricated titania woodpile structures. Similarly to the above, we calculated partial photonic bandgap positions for angles of 16° and 35.5° and for XUL and XWK directions (see Table 1).

Table 1. Partial photonic bandgap edges (nm) for woodpile structures with lateral periods between 990 nm and 1300 nm for specific angles in XUL and XWK directions

Direction	Angle, °	Calculated partial photonic bandgap edges, nm			
		990 nm	1090 nm	1190 nm	1300 nm
Along X-U-L	16	2025.8	2126.0	2231.8	2337.3
		2121.3	2221.3	2330.1	2435.8
	35.5	1912.3	1998.5	2095.1	2186.3
		1977.6	2085.7	2206.6	2320.2
Along X-W-K	16	2016.7	2116.9	2224.7	2330.2
		2120.4	2220.4	2333.8	2439.5
	35.5	1848.0	1936.4	2031.1	2127.0
		1939.3	2040.1	2159.3	2268.4

Figure 5f shows the measured reflectance spectra for these structures collected using FTIR for a wavelength range between 1.2 µm and 4.0 µm. Vertical dash lines represent the calculated photonic bandgap positions for a range of angles between 16° and 35.5°. We observe a good agreement between the expected partial bandgaps and the position of the reflectance band.
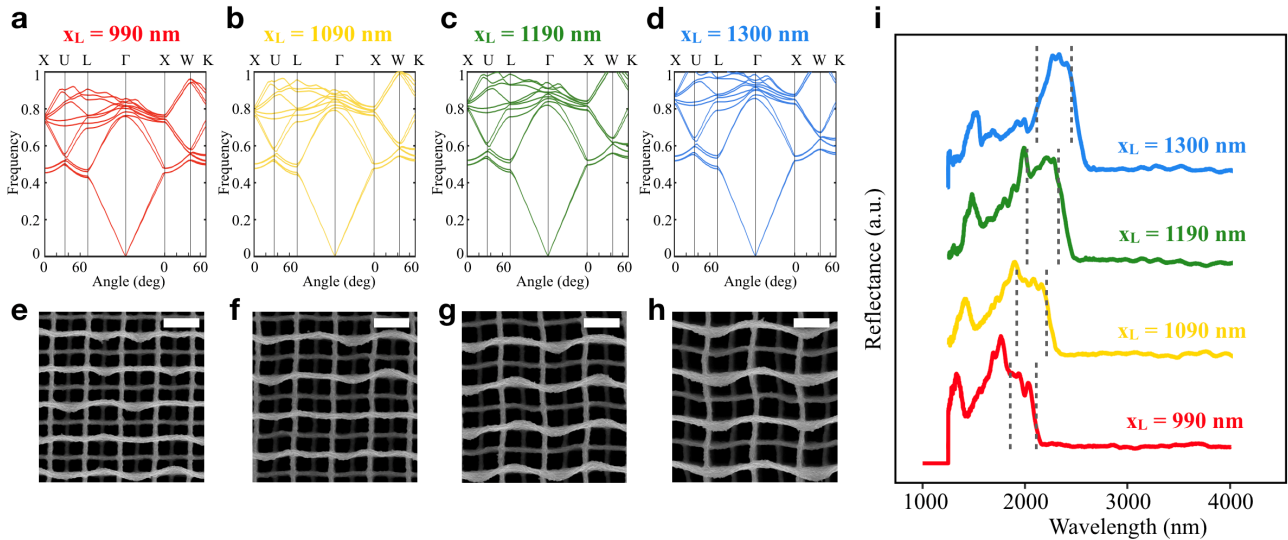

Figure 5. (a-d) Band structures of the woodpile architectures with lateral periods of 990 nm, 1090 nm, 1190 nm, and 1300 nm showing passive tuning of the partial gap position. (e-h) SEM images of representative woodpile structures (top view) fabricated using this AM process. (i) Measured reflectance spectra for as-fabricated woodpile structures with varying periodicities showing passive tuning of the reflectance band position. Vertical dash lines correspond to the range of reflectance band positions from PWE simulations for the range of angles probed by FTIR. Scale bars are 1 µm for (e-h).

4. DISCUSSION

In summary, we have developed an additive manufacturing process for titanium dioxide (TiO_2) that can produce complex 3D architectures out of rutile titania with sub-micron resolution. We have demonstrated this process by fabricating titania woodpile fct structures with partial photonic bandgaps centered at a range of wavelengths between 1.7 µm and 2.3 µm. We have shown a good agreement between FTIR reflectance spectra taken from the structures and PWE simulations. Nano-scale AM of titania has a potential to enable fast prototyping of dielectric photonic crystals in the visible and in the infrared ranges of the spectrum.

ACKNOWLEDGEMENTS

REFERENCES

[1]   Susumu Noda, Katsuhiro Tomoda, Noritsugu Yamamoto and Alongkarn Chutinan., "Full Three-Dimensional Photonic Bandgap Crystals at Near-Infrared Wavelengths," Science (80-.). **289**(5479), 604–606 (2000).

[2]   Staude, I., Thiel, M., Essig, S., Wolff, C., Busch, K., von Freymann, G. and Wegener, M., "Fabrication and characterization of silicon woodpile photonic crystals with a complete bandgap at telecom wavelengths.," Opt. Lett. **35**(7), 1094–1096 (2010).

[3]   Luo, C., Johnson, S. G. and Joannopoulos, J. D., "All-angle negative refraction in a three-dimensionally periodic photonic crystal," Appl. Phys. Lett. **81**(13), 2352–2354 (2002).

[4]   Frölich, A., Fischer, J., Zebrowski, T., Busch, K. and Wegener, M., "Titania woodpiles with complete three-dimensional photonic bandgaps in the visible," Adv. Mater. **25**(26), 3588–3592 (2013).

[5]   Ho, K. M., Chan, C. T., Soukoulis, C. M., Biswas, R. and Sigalas, M., "Photonic band gaps in three dimensions: New layer-by-layer periodic structures," Solid State Commun. **89**(5), 413–416 (1994).

[6]   Chernow, V. F., Ng, R. C. and Greer, J. R., "Designing core-shell 3D photonic crystal lattices for negative refraction," Proc. SPIE **10112** (2017).

[7]   Takahashi, S., Suzuki, K., Okano, M., Imada, M., Nakamori, T., Ota, Y., Ishizaki, K. and Noda, S., "Direct creation of three-dimensional photonic crystals by a top-down approach," Nat. Mater. **8**(9), 721–725 (2009).

[8]   Aoki, K., Guimard, D., Nishioka, M., Nomura, M., Iwamoto, S. and Arakawa, Y., "Coupling of quantum-dot light emission with a three-dimensional photonic-crystal nanocavity," Nat. Photonics **2**(11), 688–692 (2008).

[9]   Padolskytė, V., Gailevičius, D., Mikoliūnaitė, L., Katkus, T., Padolskytė, V., Gailevičius, D., Jonušauskas, L., Katkus, T., Gadonas, R., Šakirzanovas, S., Mizeikis, V., Staliunas, K. and Juodkazis, S., "3D opto-structuring of ceramics at nanoscale," Proc. SPIE **10675** (2018).

[10]   Jonušauskas, L., Gailevičius, D., Mikoliunaite, L., Sakalauskas, D., Šakirzanovas, S., Juodkazis, S. and Malinauskas, M., "Optically clear and resilient free-form μ-optics 3D-printed via ultrafast laser lithography," Materials (Basel). **10**(1), 1–18 (2017).

[11]   Yeh, C. C., Liu, H. C., Heni, W., Berling, D., Zan, H. W. and Soppera, O., "Chemical and structural investigation of zinc-oxo cluster photoresists for DUV lithography," J. Mater. Chem. C (2017).

[12]   Malinauskas, M., Ukauskas, A., Purlys, V., Gaidukeviiut, A., Baleviius, Z., Piskarskas, A., Fotakis, C., Pissadakis, S., Gray, D., Gadonas, R., Vamvakaki, M. and Farsari, M., "3D microoptical elements formed in a photostructurable germanium silicate by direct laser writing," Opt. Lasers Eng. **50**(12), 1785–1788 (2012).

[13]   Yu, S.-Y., Schrodj, G., Mougin, K., Dentzer, J., Malval, J.-P., Zan, H.-W., Soppera, O. and Spangenberg, A., "Direct Laser Writing of Crystallized TiO2 and TiO2/Carbon Microstructures with Tunable Conductive Properties," Adv. Mater. **30**(51), 1805093 (2018).

[14]   Vyatskikh, A., Kudo, A., Delalande, S. and Greer, J. R., "Additive manufacturing of polymer-derived titania for one-step solar water purification," Mater. Today Commun. **15**(March), 288–293 (2018).

[15]   Vyatskikh, A., Delalande, S., Kudo, A., Zhang, X., Portela, C. M. and Greer, J. R., "Additive manufacturing of 3D nano-architected metals," Nat. Commun. **9**(1), 593 (2018).